14th International Symposium on Turbulence and Shear Flow Phenomena (TSFP14)
Heidelberg, Germany, July 28–31, 2026

SURFACE ROUGHNESS AND INTAKE FLOW EFFECTS ON FILM FORMATION AND EVAPORATION IN METHANOL PORT FUEL INJECTION FOR MARINE ENGINES

Jannick Erhard
Reactive Flows and Diagnostics
Technical University of Darmstadt
Otto-Berndt-Str. 3, 64287 Darmstadt, Germany
erhard@rsm.tu-darmstadt.de

İrem Alp
Reactive Flows and Diagnostics
Technical University of Darmstadt
Otto-Berndt-Str. 3, 64287 Darmstadt, Germany
alp@rsm.tu-darmstadt.de

Sandra Schary
Reactive Flows and Diagnostics
Technical University of Darmstadt
Otto-Berndt-Str. 3, 64287 Darmstadt, Germany

Andreas Dreizler
Reactive Flows and Diagnostics
Technical University of Darmstadt
Otto-Berndt-Str. 3, 64287 Darmstadt, Germany
dreizler@rsm.tu-darmstadt.de

Benjamin Böhm
Reactive Flows and Diagnostics
Technical University of Darmstadt
Otto-Berndt-Str. 3, 64287 Darmstadt, Germany
boehm@rsm.tu-darmstadt.de

ABSTRACT

The application of green methanol as fuel for marine engine retrofits offers a promising pathway toward substantial greenhouse gas emission reductions. However, methanol's high enthalpy of vaporization promotes wall film formation during port fuel injection, adversely affecting mixture formation, combustion stability, and emissions. This study investigates the influence of surface roughness and intake air mass flow on liquid film formation and evaporation using a downscaled, optically accessible flow bench model of a marine engine intake port.

Time-resolved wall film measurements were performed with the refractive index matching (RIM) technique on roughened PMMA surfaces of varying roughness. Methanol injection was compared with isooctane as a conventional reference fuel under identical operating conditions. The experiments reveal pronounced differences in film dynamics: methanol shows faster film buildup and significantly longer persistence. Film evolution is governed by the combined effects of spray impingement, capillary-driven roughness invasion, aerodynamic shear, and evaporation.

Increasing intake air mass flow accelerates film decay by enhancing convective evaporation and shear-induced film removal, while higher roughness increases liquid storage capacity and prolongs film residence time. Additional RIM measurements in the combustion chamber show that higher intake mass flow also promotes liquid fuel transport into the chamber despite increased evaporation.

The results provide insight into methanol wall film behavior during port fuel injection and highlight the critical role of surface roughness and intake flow in fuel transport, evaporation, and mixture formation in methanol-fueled marine engines.

Introduction

The maritime sector accounts for approximately 3 % of global CO_2 emissions, with increasing emissions driven by international trade. To meet the Paris Agreement targets, the International Maritime Organization (IMO) aims to reduce greenhouse gas emissions by at least 70 % till 2050 compared to 2008 levels Kondratenko *et al.* (2025). Given the limited feasibility of battery-electric propulsion for deep-sea shipping and the long lifetime of vessels, retrofitting existing fleets with low- or net-zero-emission fuels is essential. Green methanol (CH_3OH) is considered a promising retrofit option Kondratenko *et al.* (2025). It can be handled and stored as a liquid under ambient conditions and is compatible with established marine engine technologies. Compared to hydrogen, methane, or ammonia, methanol poses fewer storage and infrastructure challenges. Additional advantages include lower adiabatic flame temperatures reducing NO_x emissions, the absence of sulfur eliminating SO_x, and high knock resistance.

However, methanol exhibits a high enthalpy of vaporization and a lower heating value ($H_\mathrm{i} = 15.8\,\frac{\mathrm{kJ}}{\mathrm{mL}}$) compared to diesel ($H_\mathrm{i} = 35.8\,\frac{\mathrm{kJ}}{\mathrm{mL}}$), requiring higher injected volumes. Both properties increase the tendency for liquid wall film formation during injection, which can impair mixture formation and affect combustion stability and emissions Güdden *et al.* (2021). Port fuel injection of methanol represents the most straightforward retrofit strategy. The present study therefore investigates

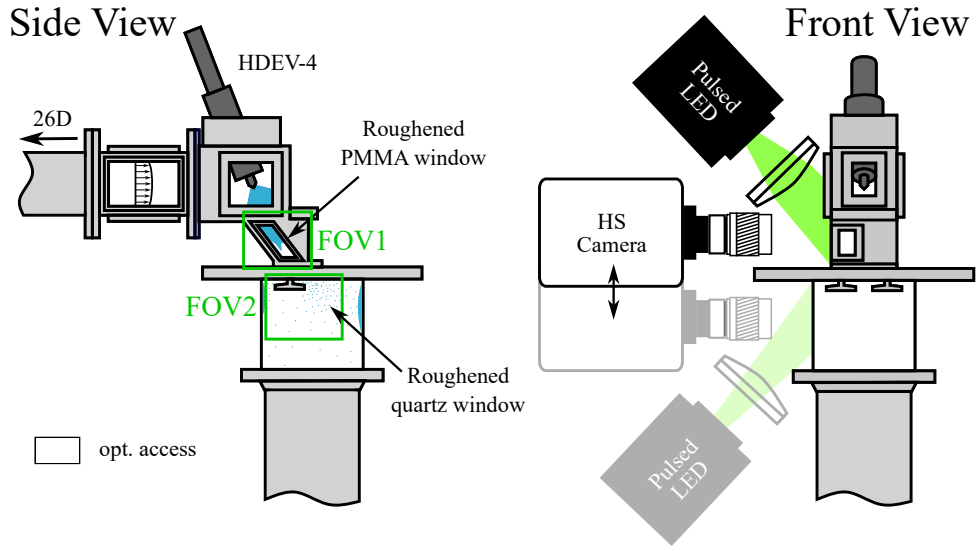

Figure 1: Sketch of the optically accessible flow bench and the experimental setup used for the refractive index matching (RIM) experiments. The second setup used for the investigation in the combustion chamber is shown faded.

wall film formation as a function of surface roughness and intake air mass flow using a downscaled, optically accessible flow bench model of a marine engine. Methanol is compared to a conventional reference fuel, and the transport of liquid droplets into the combustion chamber is analyzed.

Wall films formed after spray impingement are highly transient and spatially inhomogeneous, typically occurring at micrometer-scale thicknesses. Their formation and evaporation depend strongly on local flow and surface conditions, necessitating spatially and temporally resolved, non-intrusive diagnostics. Among established optical techniques such as laser-induced fluorescence (LIF) Jüngst & Kaiser (2021), UV absorption Shway *et al.* (2023), and RIM Drake *et al.* (2003), the latter is most suitable for the present setup due to limited optical access, complex geometry, and rough surfaces.

Experimental setup

Marine engine flow bench

The optically accessible flow bench is shown in Figure 1. A 26D long inlet channel is used to generate a fully developed turbulent flow into the flow geometry of a marine engine intake port, scaled down by a factor of $\sqrt{13}$. The air mass flow $\dot{M}$ is provided using a mass flow controller. For the methanol injection, a Bosch HDEV-4 injector is utilized. It is operated to mimic an engine speed of 500 RPM resulting in an injection frequency of $f_{\mathrm{inj}} = 4.167\,\mathrm{Hz}$ at an injection pressure of $p_{\mathrm{inj}} = 50\,\mathrm{bar}$. The injection length was set to $t_{\mathrm{inj}} = 15\,\mathrm{ms}$. Optical access to the intake port is provided by custom-made PMMA windows, which preserve the original port geometry. Through the two fixed intake valves, the fuel then enters the optically accessible combustion chamber of the flow bench. In order to facilitate the monitoring of the boundary conditions, the flow bench has been equipped with thermocouples at strategic locations to measure the temperature 0.5 mm beneath the surface.

Refractive Index Matching

For time-resolved, two-dimensional determination of wetted area and local fuel film thickness, RIM was applied at different locations of the flow bench Drake *et al.* (2003).

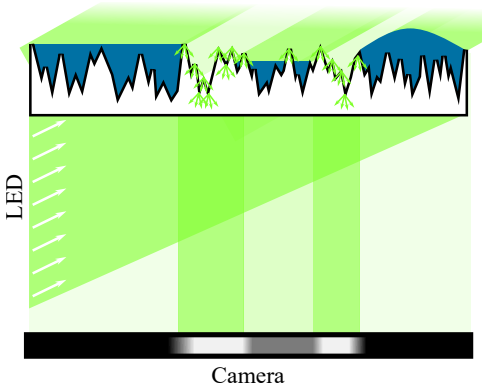

Figure 2: Schematic representation of the RIM principle. Illumination under an oblique angle leads to strong diffuse scattering from dry rough surfaces, whereas filling of the roughness cavities with liquid suppresses back-scattering and results in darker image regions. The recorded intensity is related to the local liquid volume within the surface roughness.

The method requires a roughened transparent substrate, here PMMA. When illuminated under an oblique angle, light is diffusely scattered at the roughness cavities due to the refractive-index gradient between air and substrate, causing the dry surface to appear bright. If a liquid with a refractive index close to that of the substrate is applied, it fills the cavities, reduces back-scattering, and the wetted regions appear darker. The contrast therefore allows differentiation between varying local film thicknesses.

The working principle is shown in Figure 2. Since the signal depends on the roughness, complete filling of the cavities leads to saturation. The maximum resolvable film thickness is therefore linked to the characteristic roughness R_a, and films exceeding the roughness amplitude cannot be distinguished.

Three roughness levels were generated by sandblasting ($R_a = 10\,\mu\mathrm{m}$ and $R_a = 5.5\,\mu\mathrm{m}$) or sandpaper treatment ($R_a = 1\,\mu\mathrm{m}$). Surface roughness was determined using a MarSurf PD10 ($\pm 8\,\%$ uncertainty). Measurements were performed in the intake port (*FOV1*) and combustion chamber (*FOV2*), see

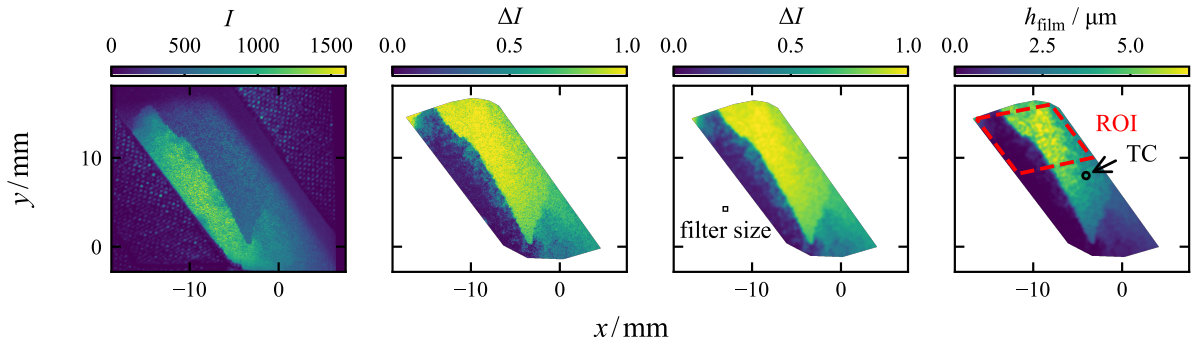

Figure 3: Processing steps for the RIM method. From left to right: Dewarped raw image, ΔI image, filtered ΔI image using a Gaussian kernel with $\sigma = 0.2\,\mathrm{mm}$ and calibrated image with the used region of interest (ROI) marked in red. The position of the used thermocouple, installed on the opposite intake port, is marked with a black circle.

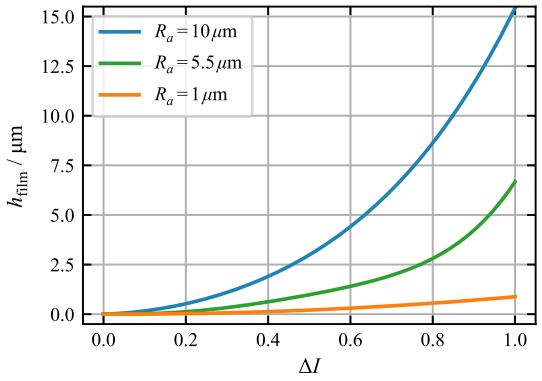

Figure 4: Polynomial fits used for calibration for different R_a.

Figure 1. Illumination was provided by a pulsed LED (*ILA LPS III*, 50 µs pulse length), and images were recorded with a high-speed camera (*Phantom TMX 7510*, 200 Hz, 100 mm lens).

Image processing followed the workflow in Figure 3. Optical distortions were corrected using a third-order polynomial transformation based on a dot-pattern calibration target attached to the curved window. After cropping to the valid signal region, the parameter ΔI was calculated as

$$\Delta I = \left(1 - \frac{I}{I_{\mathrm{bkg}}}\right) \cdot \frac{1}{C_{\mathrm{liq}}}, \tag{1}$$

where I denotes the raw intensity and I_{bkg} the mean background image of the dry surface. The correction factor C_{liq} accounts for differences in refractive index between liquid and PMMA ($n = 1.49$). For methanol ($n = 1.32$), $C_{\mathrm{methanol}} = 0.77$, and for isooctane ($n = 1.39$), $C_{\mathrm{isooctane}} = 0.88$. The factors were determined empirically using films exceeding the roughness amplitude. To reduce fixed-pattern noise from the surface structure, images were filtered with a Gaussian kernel ($\sigma = 0.2\,\mathrm{mm}$).

Finally, ΔI was converted to film thickness h_{film} using a calibration approach similar to Ding *et al.* (2018). The resulting calibration polynomials (see Figure 4) demonstrate that surface roughness affects both dynamic range and sensitivity.

It should be noted that RIM provides a two-dimensional, surface-integrated measure of liquid volume and does not resolve the true three-dimensional film topology on the rough surface. For simplicity, the term film thickness is used in the following.

Results and Discussion

The RIM technique was used to investigate film development during repeated injections in the intake port of a port fuel injected marine engine. In addition, wall temperature was measured at the same axial position on the opposite side of the flow geometry using a thermocouple installed 0.5 mm below the surface (see Figure 3). Each measurement cycle consisted of five consecutive injections to establish a continuous wall film, followed by a waiting period until complete evaporation. The scheme was repeated ten times, ensuring a stabilized wall temperature of $T_{\mathrm{wall}} = 20\,^{\circ}\mathrm{C}$ prior to each run.

The temporal evolution of the wall film during a representative injection cycle is shown in Figure 5 for methanol at $\dot{M} = 150\,\frac{\mathrm{kg}}{\mathrm{h}}$ and $R_a = 5.5\,\mu\mathrm{m}$. An optical artifact occurs in the lower half of the image due to diffuse back scattering and is excluded from quantitative evaluation. Immediately after the first injection ($t = 20\,\mathrm{ms}$), a highly non-uniform film distribution forms due to direct spray impingement. Subsequently, local film thickness decreases owing to evaporation and shear removal, while thicker liquid structures transported from upstream regions spread along the wall ($t = 180\,\mathrm{ms}$). Dry regions ahead of these thick films dry out due to evaporation and reduced capillary driving forces slowing down the spreading of the thick films. After the second injection ($t = 320\,\mathrm{ms}$), the wall is rewetted and the transported films continue spreading. With subsequent injections, a continuous film develops and the RIM signal saturates. Following the final injection, the film gradually recedes ($t = 1500\,\mathrm{ms}$ to $1900\,\mathrm{ms}$), with spatially varying decay rates governed by local flow conditions.

For quantitative comparison, film thickness was spatially averaged over a defined ROI excluding the artifact region and ensemble averaged over ten cycles, yielding $\overline{h}_{\mathrm{film}}$ and its standard deviation.

Figure 6 shows $\overline{h}_{\mathrm{film}}$ over time t for methanol and isooctane at $\dot{M} = 150\,\frac{\mathrm{kg}}{\mathrm{h}}$ and $R_a = 5.5\,\mu\mathrm{m}$. Injection events appear as sharp peaks (black arrows).

Immediately after the first injection, methanol forms a thicker film than isooctane due to reduced evaporation during injection and consequently a larger impinging liquid frac-

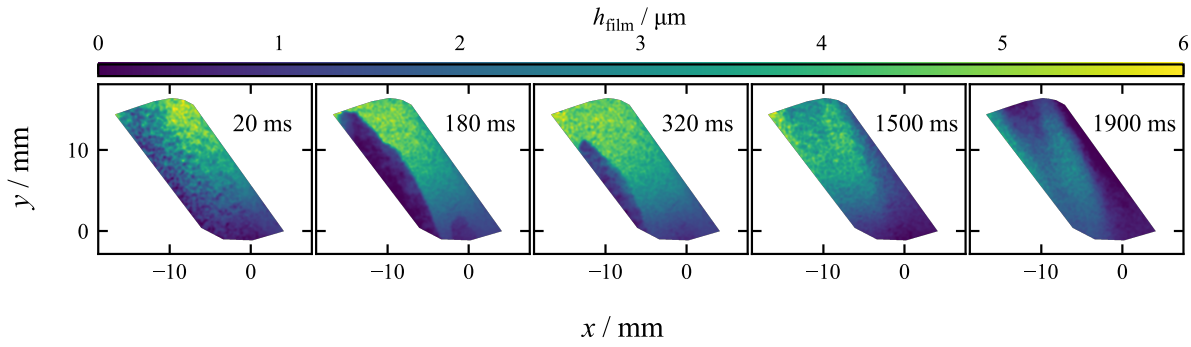

Figure 5: Time-resolved evolution of the methanol wall film during one injection cycle for $\dot{M} = 150\,\frac{\mathrm{kg}}{\mathrm{h}}$ and $R_a = 5.5\,\mu\mathrm{m}$. From left to right: initial spray impingement (1), spreading of the liquid film (2–3), re-wetting of the wall due to the second injection (3), and subsequent film decay (4–5).

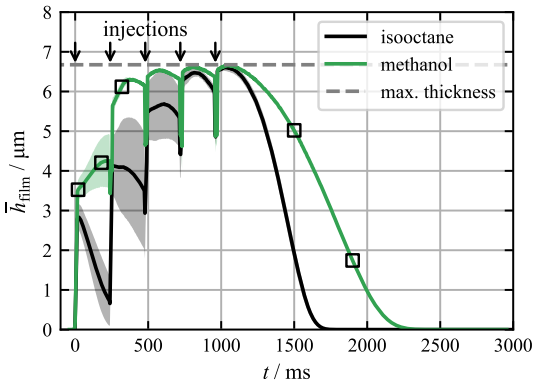

Figure 6: $\overline{h}_{\mathrm{film}}$ as a function of t for isooctane (black) and methanol (green) at $\dot{M} = 150\,\frac{\mathrm{kg}}{\mathrm{h}}$ for $R_a = 5.5\,\mu\mathrm{m}$. Solid lines indicate the mean values, while the shaded regions represent the standard deviation. The time of the five injection within a cycle are marked by black arrows. The black squares corresponded to the time steps shown in Figure 5.

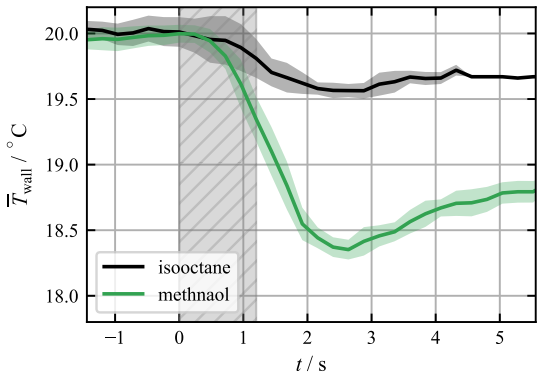

Figure 7: $\overline{T}_{\mathrm{wall}}$ as a function of t for isooctane (black) and methanol (green) at $\dot{M} = 150\,\frac{\mathrm{kg}}{\mathrm{h}}$. Solid lines indicate the mean values, while the shaded regions represent the standard deviation. The shaded gray area indicates the time interval during which fuel is injected.

tion. In contrast to isooctane, methanol exhibits continued film growth after the first injection caused by the transport of accumulated liquid from other regions. Isooctane films primarily evaporate without forming thick structures.

Methanol reaches signal saturation earlier and shows lower cycle-to-cycle variation, indicating more stable and persistent film formation. After the fifth injection ($t \approx 1000\,\mathrm{ms}$), the isooctane film decays considerably faster than the methanol film, consistent with its lower enthalpy of vaporization ($\Delta H_{\mathrm{vap,isooctane}} = 220\,\frac{\mathrm{J}}{\mathrm{mL}}$ vs. $\Delta H_{\mathrm{vap,methanol}} = 870\,\frac{\mathrm{J}}{\mathrm{mL}}$).

This difference is also reflected in the measured wall temperature (see Figure 7), where methanol induces a significantly stronger cooling after injection.

During individual injections, $\overline{h}_{\mathrm{film}}$ temporarily decreases due to spray–film interaction. High spray momentum entrains and redistributes the pre-existing film, reducing local thickness. After injection, roughness cavities are gradually refilled by slower lateral transport until a saturated state is reached. The decay of the signal immediately after injection suggests that the majority of evaporation takes place within the roughness cavities.

In Figure 8, the influence of air mass flow on the methanol film is shown. In contrast to Figure 6, only the film evolution after the last injection is considered. The reference time $t_{90\,\%}$ is defined as the instant when the spatially averaged film thickness $\overline{h}_{\mathrm{film}}$ reaches 90 % of the maximum distinguishable thickness h_{max,R_a}. This threshold provides a reproducible reference close to saturation while remaining within the non-saturated regime of the RIM signal.

The subsequent decay of the film is plotted as a function of $t - t_{90\,\%}$ for $\dot{M}$ between $50\,\frac{\mathrm{kg}}{\mathrm{h}}$ and $250\,\frac{\mathrm{kg}}{\mathrm{h}}$ at $R_a = 5.5\,\mu\mathrm{m}$. Higher mass flow rates clearly result in faster film decay. The average evaporation rate $\dot{h}_{\mathrm{film}}$ increases approximately linearly with $\dot{M}$ ($R^2 = 0.98$), indicating enhanced heat and mass transfer. This trend is also reflected in the stronger and faster wall temperature decrease at higher $\dot{M}$ (Figure 9). However, the enhanced cooling cannot be attributed to evaporation alone. Increasing $\dot{M}$ raises the Reynolds number and thus the convective heat transfer coefficient, enhancing wall cooling. Additionally, shear-driven transport can deliver larger amounts of liquid to the measurement location, increasing local evaporative cooling. Both effects superimpose, leading to the pronounced temperature drop at higher mass flow rates.

Beyond their thermal impact, increased aerodynamic shear accelerates film removal. The delay between the end of injection t_{EOI} and $t_{90\,\%}$ decreases with increasing $\dot{M}$. This

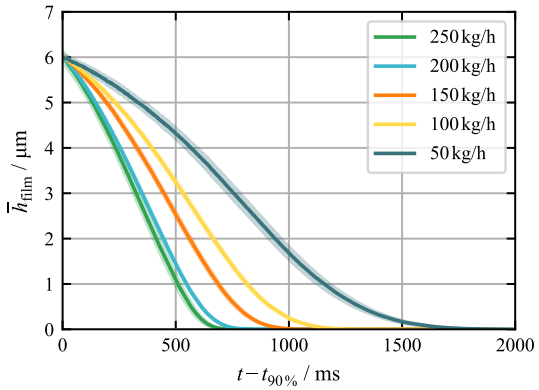

Figure 8: Evolution of $\overline{h}_{\text{film}}$ after the time where it has decreased to 90 % as a function of $t - t_{90\%}$ for different $\dot{M}$ at $R_a = 5.5\,\mu\text{m}$. Lines indicate the mean values, while the shaded regions represent the standard deviation.

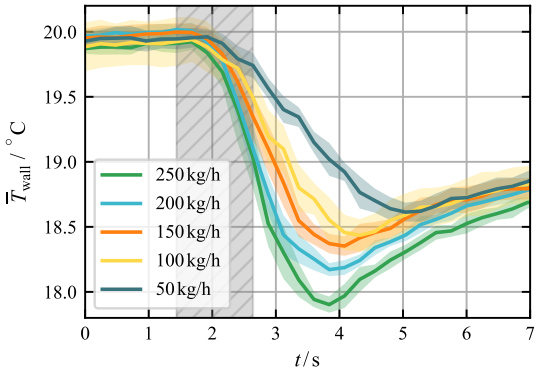

Figure 9: The evolution off the wall temperature $\overline{T}_{\text{wall}}$ for a variation of $\dot{M}$. Lines indicate the mean values, while the shaded regions represent the standard deviation. The shaded gray area indicates the time interval during which methanol is injected.

indicates that higher shear forces more effectively remove liquid from the wall, particularly above the roughness. Together with enhanced evaporation, this results in significantly faster film decay at elevated mass flow rates.

Since most evaporation occurs within the surface roughness, its influence was investigated. Surface roughness affects both evaporation behavior and measurement characteristics. Lower roughness increases RIM sensitivity but leads to earlier saturation due to the smaller roughness volume.

Figure 10 shows $\overline{h}_{\text{film}}$ at $\dot{M} = 150\,\frac{\text{kg}}{\text{h}}$ for three roughness levels. For $R_a = 1\,\mu\text{m}$, the signal saturates after the first injection, reflecting the limited roughness volume. For $R_a = 5.5\,\mu\text{m}$ and $R_a = 10\,\mu\text{m}$, the initial film thickness is nearly identical, confirming calibration consistency. At later times, differences emerge. For $R_a = 5.5\,\mu\text{m}$, an increase in $\overline{h}_{\text{film}}$ occurs due to transport of thick liquid structures along the wall. This behavior is absent for $R_a = 10\,\mu\text{m}$, suggesting that the film thickness relative to roughness amplitude is insufficient for large-scale liquid redistribution between cavities.

Higher roughness levels require more injections to reach saturation due to the larger roughness volume. After the final injection, films on surfaces with higher roughness exhibit a

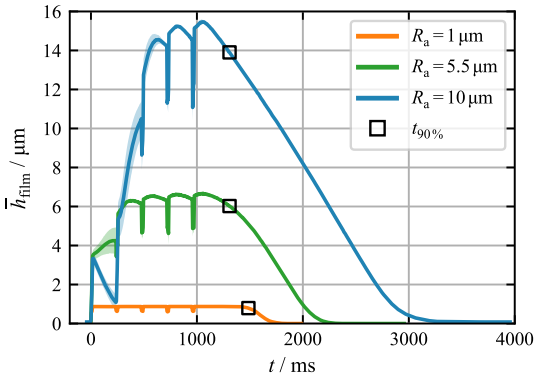

Figure 10: Evolution of the spatially averaged methanol film thickness $\overline{h}_{\text{film}}$ at a mass flow rate of $\dot{M} = 150\,\frac{\text{kg}}{\text{h}}$ for different surface roughness levels R_a. Square markers indicate the time at which $\overline{h}_{\text{film}}$ falls below 90 % of the maximum distinguishable film thickness h_{max,R_a} for the respective roughness. Solid lines represent the ensemble-averaged values, while the shaded regions denote the corresponding standard deviations.

longer decay, owing to the larger liquid volume retained within the roughness that must evaporate. When considering the onset time $t_{90\%}$, representing confinement of liquid primarily within the roughness cavities, only minor differences between $R_a = 5.5\,\mu\text{m}$ and $R_a = 10\,\mu\text{m}$ are observed. For $R_a = 1\,\mu\text{m}$, this transition occurs slightly later, indicating that a comparatively larger fraction of liquid resides above the roughness and must first be removed by shear before evaporation within the cavities dominates.

Since shear-induced removal of wall films does not directly enhance methanol evaporation and thus does not improve mixture formation, the transport of liquid methanol into the combustion chamber as a function of intake air mass flow is of particular interest.

To investigate this effect, the RIM method was additionally applied to the combustion chamber wall (FOV2 in Figure 1). The quartz glass liner was sandblasted to obtain a surface roughness of $R_a = 3\,\mu\text{m}$. No calibration was performed, as unrealistically low wall temperatures prevent a meaningful quantitative interpretation of absolute film thicknesses. Therefore, the following analysis focuses on qualitative film topology and relative trends with varying $\dot{M}$. All other processing steps were identical to those used for the intake port measurements.

Figure 11 shows ΔI images at $t = 120\,\text{ms}$ after a single injection for different air mass flow rates. The intake valve position is marked in the upper left corner by a white dashed outline. The liquid film forms predominantly near the valve and is transported downstream along the liner by the airflow. With increasing $\dot{M}$, the wetted area increases, despite the generally higher evaporation rates at elevated mass flow. Larger regions of saturated ΔI indicate thicker films at higher $\dot{M}$, suggesting that more liquid methanol reaches the combustion chamber. This behavior results from the combined effects of increased airflow momentum, enhanced droplet entrainment, reduced droplet residence time limiting evaporation during transport, and stronger shear-driven removal of liquid from upstream walls. These observations are consistent with trends identified in the intake port. In addition, fingering instabilities become more pronounced at higher $\dot{M}$. Such instabilities are promoted

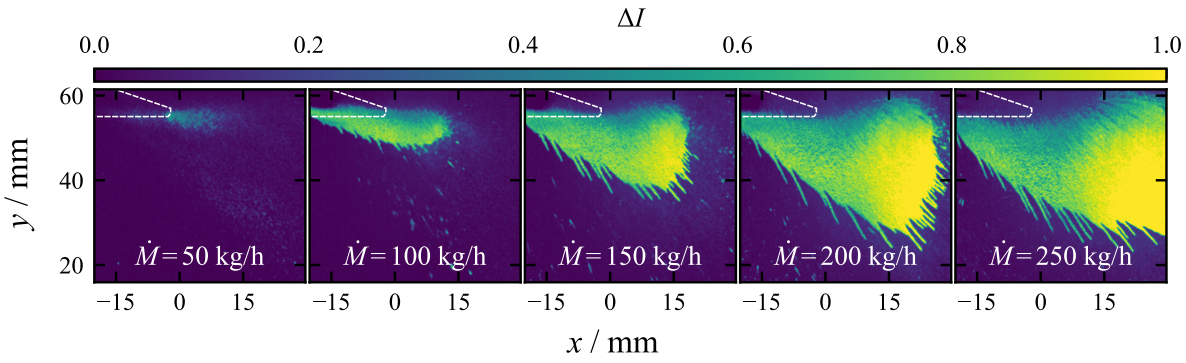

Figure 11: The influence of $\dot{M}$ on the wall film formation on the liner of the combustion chamber. Indicating the amount non evaporated, liquid methanol that is transported into the combustion chamber. The position of the valve is marked with dotted lines.

by thicker films and elevated shear forces Ma & Liu (2021), both of which increase with $\dot{M}$. Their occurrence therefore provides further qualitative evidence of enhanced liquid fuel transport into the combustion chamber. Although higher $\dot{M}$ enhances evaporation, the present results indicate that its influence on transport mechanisms dominate under the investigated conditions. Thus, increasing $\dot{M}$ shifts the balance toward transport-driven liquid penetration into the combustion chamber rather than complete upstream evaporation. Despite the qualitative nature of this analysis, the consistency across operating conditions supports the robustness of this interpretation.

Conclusions

In this study, the formation, transport, and evaporation of liquid fuel films during port fuel injection were investigated for methanol and isooctane using an optically accessible flow bench. Particular emphasis was placed on the influence of surface roughness and intake air mass flow, as both parameters are critical for methanol-fueled marine engine retrofits.

Pronounced differences in wall film behavior were observed between methanol and isooctane. Due to its high enthalpy of vaporization, methanol exhibits faster film buildup and significantly longer persistence on the wall. The film evolution results from the interplay of spray impingement, capillary-driven transport within the surface roughness, aerodynamic shear forces, and evaporation. The study shows that a substantial fraction of the liquid is retained within the roughness, where evaporation dominates over shear-induced removal. Surface roughness strongly influences both liquid storage capacity and decay dynamics. Higher roughness increases the available roughness volume and prolongs film residence time, while suppressing large-scale liquid transport along the wall. In contrast, lower roughness levels saturate rapidly and exhibit faster film removal. Increasing intake air mass flow accelerates film decay through enhanced convective evaporation and shear-driven erosion outside the roughness cavities. Simultaneously, higher mass flow promotes liquid fuel transport into the combustion chamber, despite increased evaporation, indicating that shear-induced removal does not necessarily improve mixture formation.

Overall, the results provide new insight into methanol wall film dynamics under port fuel injection conditions and highlight the critical role of surface roughness and intake flow on the fuel evaporation and mixture formation.

ACKNOWLEDGMENT

This research is funded by the German Federal Ministry for Economic Affairs and Climate Action on the basis of a decision by the German Bundestag (project no. 03SX585B), which is gratefully acknowledged. In this context, the authors would like to thank the CliNeR-EC0 project partners, Everllence and WTZ-Roßlau gGmbH, for their collaboration and support.

We kindly acknowledge generous support by Deutsche Forschungsgemeinschaft through SFB-Transregio 150 Project Number 237267381-TRR150.

REFERENCES

Ding, Carl-Philipp, Sjöberg, Magnus, Vuilleumier, David, Reuss, David L., He, Xu & Böhm, Benjamin 2018 Fuel film thickness measurements using refractive index matching in a stratified-charge si engine operated on e30 and alkylate fuels. *Experiments in Fluids* **59** (3), 133.

Drake, M.C., Fansler, T.D., Solomon, A.S. & Szekely, G.A. 2003 Piston films as a source of smoke and hydrocarbon emissions from a wall-controlled spark-ignited direct-injection engine (sae paper 2003-01-0547). *SAE Trans J Engines* **112**, 762–783.

Güdden, Arne, Pischinger, Stefan, Geiger, José, Heuser, Benedikt & Müther, Martin 2021 An experimental study on methanol as a fuel in large bore high speed engine applications – port fuel injected spark ignited combustion. *Fuel* **303**, 121292.

Jüngst, N. & Kaiser, S.A. 2021 Visualization of soot formation from evaporating fuel films by laser-induced fluorescence and incandescence. *Proceedings of the Combustion Institute* **38** (1), 1089–1097.

Kondratenko, A.A., Zhang, M. & Tavakoli, S. 2025 Existing technologies and scientific advancements to decarbonize shipping by retrofitting. *Renewable and Sustainable Energy Reviews* .

Ma, Chao & Liu, Jianshe 2021 Thin-film evolution and fingering instability of self-rewetting films flowing down an inclined plane. *Physics of Fluids* **33** (2), 022101.

Shway, Kamal, Jüngst, Niklas, Bardi, Michele, Bruneaux, Gilles & Kaiser, Sebastian A. 2023 A multispectral uv–vis absorption technique for quantitative high-speed field-sequential imaging of fuel films and soot in combustion. , vol. 39, pp. 1475–1483.